Journal of Catalysis 279 (2011) 397–402

Contents lists available at ScienceDirect

Journal of Catalysis

journal homepage: www.elsevier.com/locate/jcat

Direct observation of catalyst behaviour under real working conditions with X-ray diffraction: Comparing SAPO-18 and SAPO-34 methanol to olefin catalysts

David S. Wragg [a,*], Duncan Akporiaye [b], Helmer Fjellvåg [a]

[a] inGAP Centre for Research Based Innovation, Centre for Materials Science and Nanotechnology and Department of Chemistry, University of Oslo, P.O. Box 1033 Blindern, N-0315 Oslo, Norway
[b] SINTEF Materials and Chemistry Forskningsvn 1, N-0314 Oslo, Norway

ARTICLE INFO

Article history:
Received 12 November 2010
Revised 1 February 2011
Accepted 27 February 2011
Available online 29 March 2011

Keywords:
Heterogeneous catalysis
X-ray diffraction
Zeolites
Methanol to olefins

ABSTRACT

We have made direct observations of the behaviour of the silicoaluminophosphate framework of the SAPO-18 catalyst under working conditions in the methanol to olefin conversion process. Time-resolved synchrotron powder X-ray diffraction data for the process at 450 °C show that the unit cell of the catalyst expands by around 0.9%, significantly less than the structurally similar SAPO-34. The smaller expansion is explained in terms of the cage volume and the rigidity of the structure compared with SAPO-34. Expansion is caused by the build-up of "hydrocarbon pool" intermediates in the cages. The lack of expansion and hence slower build-up of large hydrocarbons is linked to the slower deactivation of SAPO-18 compared with that of SAPO-34. The mechanism for suppressing the formation of the large polycyclic aromatics associated with the deactivation of SAPO MTO catalysts remains open.

1. Introduction

As oil becomes increasingly scarce and costly, the conversion of methanol to olefins becomes an attractive route to alkenes for subsequent polymerisation and other chemical processes. The starting material, methanol, is cheap and can be obtained from fossil fuel sources or biofeedstocks, making it possible to sustain olefin supply without fossil fuels. The catalysts for this reaction are acidic zeolite frameworks. ZSM-5 was the first to be applied, – producing a range of hydrocarbons from methanol [1], but more recently the silicoaluminophosphate (SAPO-*n*) zeotype frameworks have been developed as highly selective catalysts for the production of olefins [2]. SAPO-34 has widely been studied in respect of this; however, it is not the only SAPO material which is active and selective for the process. SAPO-18, first prepared by Wendelbo and characterised by Chen and co-workers [3–6], displays good activity and selectivity as well as superior lifetime to SAPO-34. It is also known to exist as an intergrowth with SAPO-34 [7,8]. The two structures are closely related. Both are built up from double six-ring units (D6Rs), i.e., two connected rings of six tetrahedral Si/Al/P atoms linked by oxygen, which are arranged in identical layers. An A-A-A stacking of the layers gives SAPO-34 (International Zeolite Association framework type CHA) while A-B-A sequence (with the B layer simply the A-type layer rotated by 180°) gives SAPO-18 (International Zeolite Association framework type AEI). AFM studies have recently revealed that these layers are in fact a basic unit of crystallisation in SAPO-34 [9].

The layers form structures with eight-ring windows (rings of eight tetrahedral atoms linked by oxygen) and large internal cages. The ordering of the D6Rs is, however, slightly different [10]. This leads to two structures with the same framework density (number of tetrahedral atoms per 1000 Å^3; 15.1 for both structures [8]) but significantly different cage shapes (Fig. 1).

The mechanism of the MTO process over SAPO-34 has been studied intensively, and several reviews are available [11,12]. The hydrocarbon pool mechanism first proposed by Dahl and Kolboe [13,14] is now generally accepted [12]. Work by Hunger et al. (using *in* and *ex situ* NMR spectroscopy) [15,16] and Marcus et al. (using *ex situ* NMR and GC analysis of the organic material from used catalysts) [17] has shown that the same mechanism governs the MTO reaction over SAPO-18. The longer active lifetime of SAPO-18 compared with that of SAPO-34 is also discussed in these articles, and the authors show that larger coke species are present in deactivated SAPO-18, with deactivation requiring more than twice the amount of methanol feed compared with SAPO-34. The kinetics of the MTO reaction over SAPO-18 were studied by Gayubo et al. [18,19] with further evidence of more prolonged catalytic activity in SAPO-18. Little, however, was known about the structural behaviour of the catalysts during the reaction until our *in situ* synchrotron powder X-ray diffraction combined with mass spectrometry and Raman spectroscopy studies of SAPO-34 under real working conditions [20,21] revealing highly asymmetric changes in the unit cell during the MTO reaction. In order to gain a better understanding of the process and its relation to crystal

* Corresponding author. Fax: +47 228 55441.
E-mail address: david.wragg@smn.uio.no (D.S. Wragg).

0021-9517/$ - see front matter © 2011 Elsevier Inc. All rights reserved.
doi:10.1016/j.jcat.2011.02.011

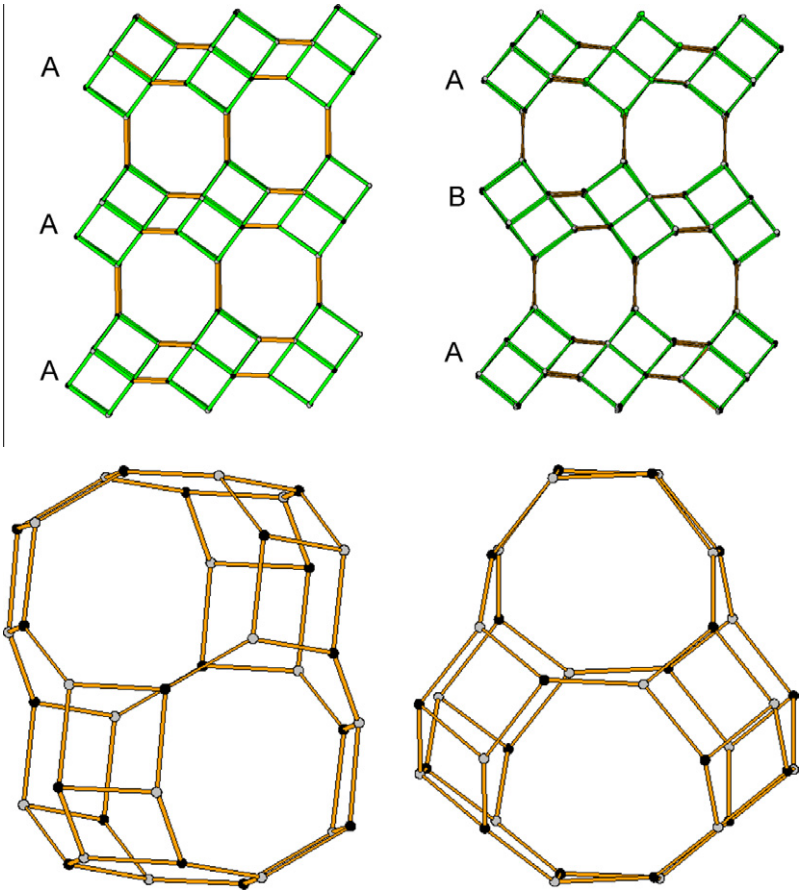

Fig. 1. Framework structures and cages of SAPO-34 (left) and SAPO-18 (right) drawn with tetrahedral Al/P/Si atoms only. The upper images show the arrangement of D6R units (coloured green) with A-A-A (SAPO-34) and A-B-A (SAPO-18) stacking of the layers. The resulting cages are shown below. (For interpretation of the references to colour in this figure legend, the reader is referred to the web version of this article.)

structure aspects, we have now applied this methodology to SAPO-18 under MTO conditions.

2. Experimental

A sample of SAPO-18 prepared according to the method of Chen et al. [4] with 8% Si (i.e. 100 × Si/(Si + P + Al)) was obtained from professor K.P. Lillerud of the University of Oslo and calcined at 550 °C for 10 h in air. The sample contains a small impurity (0.5 wt.% determined from the PXRD data) of SAPO-5. SEM images of the crystallites show a square plate-like morphology with edges of between 0.5 and 2 μm and a thickness of less than 0.5 μm. We note that differences in the nature of the acid sites observed in SAPO-18 compared with SAPO-34 are reported in literature [3,5,16,17,22], caused by differences in the mechanism of silicon incorporation into the framework. SAPO-34 with less than 8% Si contains almost exclusively silicon substituted for phosphorus while SAPO-18 with the same amount of silicon contains significant amounts of Si for Al substitution. When silicon is substituted for both Al and P, some of the Brønsted acidity is cancelled out; therefore, SAPO-18 normally contains less acid sites compared with SAPO-34 with the same level of Si substitution.

In situ synchrotron powder XRD data for SAPO-18 under MTO conversion conditions at 450 °C were collected at beamline BM01A (the Swiss Norwegian Beam Lines) of the ESRF, using a one-circle diffractometer with a MAR345 image plate detector. The wavelength was 0.70417 Å (determined from the powder pattern of NIST SRM 660a LaB_6), and the maximum 2θ angle was 35°. The sample was packed between plugs of silica wool in a 0.5-mm quartz capillary and mounted in a flow cell based on that described by Norby [23]. The sample was heated to working temperature under flowing helium (20 ml/min), and after a short period of holding at 450 °C, the flow was switched to helium bubbled through methanol (at 22 °C in the air-conditioned experimental hutch) for 3 h. The time resolution between XRD patterns was 107 s.

The diffraction images were converted into conventional 1D powder patterns with FIT2D [24,25] and scaled against beam decay. The patterns were fitted by the Le Bail [26] and Pawley [27] methods to obtain accurate unit cell parameters using both GSAS [28] and TOPAS [29]. Refinements were carried out in batch and parametric [30] modes with very similar results (parametric refinements used single-scale and zero-point parameters for all data sets). Models for Fourier analysis were obtained from a parametric Rietveld refinement of all data sets using TOPAS.

The product stream was analysed with a Pfeiffer GSD-301-O1 Omnistar mass spectrometer scanning an M/e range of 4–70 with an acquisition time of 37 s.

PXRD data on a sample reacted with methanol saturated helium in the capillary flow cell for 21 h at 450 °C were collected on a Bruker D5000 diffractometer using Cu Kα1 radiation (Ge monochromator) in capillary mode and refined using TOPAS academic.

3. Results and discussion

The unit cell dimensions of SAPO-18 vary during the MTO reaction (Fig. 2). We note a clear negative thermal expansion in

SAPO-18 while heating to the reaction temperature. This is in line with the findings of Amri and Walton for the aluminium and gallium phosphate versions of this framework [31].

The structural changes during the MTO process are of similar magnitude for all three axes (*a* contracts; *b* and *c* extend) while the monoclinic angle, β, is reduced. The overall volume of the unit cell increases by 0.9 (±0.01) %. In a sample of SAPO-34 with the same silicon content, a 3% volume increase is observed [20], with most of the expansion in the *c*-axis direction (note that the crystallographic axes of SAPO-34 and SAPO-18 do not have the same orientation with respect to the structure). The slope of the curves does reduce towards the end of the first 3-h reaction period; however, unlike SAPO-34, there is no clear end point for the unit cell parameter development. This is significant in that it may reflect the longer active lifetime of SAPO-18. Several studies have shown that crystallite size can affect activity in MTO catalysts [32–36]; however, the general conclusion is that larger crystallites should lead to longer reactant residence time on the catalyst and faster deactivation. In this case, the SAPO-18 crystallites are slightly larger (0.5–2-μm plates compared with 0.5–1-μm cubes for SAPO-34) yet the catalyst maintains its activity for longer.

Mass spectra collected during the *in situ* experiment show that there are definite differences in the activity of SAPO-18 compared with that of SAPO-34. Fig. 3 shows the mass spectra for methanol ($M/e = 31$), dimethyl ether ($M/e = 45$) and propene ($M/e = 42$) during the experiment alongside the unit cell volume variation. In SAPO-18, the production of propene does not drop to zero during the period of measurement, although estimates based on the methanol and dimethyl ether streams suggest that the overall conversion drops from 100% to zero during this period. This is in contrast to SAPO-34, which displays similar peak values of propene production for multiple cycles but with the propene production quickly dropping to zero after the peak in activity [2,20]. Both catalysts show a slight decline in dimethyl ether production over time on stream, though as for other zeolitic MTO catalysts this does not drop to zero.

We have previously shown that expansion in SAPO-34 [20] during the MTO process is strongly correlated with the build-up of reaction intermediates inside the cages. These become increasingly graphitic as the catalyst deactivates over time. Mass spectra collected during our experiments confirm that SAPO-18 remains active for longer than SAPO-34 (the catalyst still produces appreciable amounts of propene after 3 h at 450 °C, see Fig. 3). Marcus et al. compared the coke in SAPO-18 and SAPO-34 after the MTO process and showed that SAPO-18 tends to form larger polyaromatic species than SAPO-34 (pyrenes rather than phenanthrenes), this is explained by the shape of the cages in SAPO-18 allowing easier formation of the larger aromatics [17]. The simple docking studies in this paper are informative, showing that even with pyrene trapped inside there is space in the SAPO-18 cage. This observation helps to rationalise the smaller expansion observed by both *in situ* X-ray diffraction and the extended activity: SAPO-34 fills with coke, expands, becomes blocked and deactivates. SAPO-18 does not fill, despite the larger coke molecules, due to its cage shape and therefore need not expand. It may be possible to confirm this by studying the MTO reaction over catalysts such as SAPO-56 [37] (IZA framework code AFX) and SAPO versions of AlPO-52 [38,39] (IZA framework code AFT) which contain the AFT cage – an extended version of the chabazite cages of SAPO-34. This cage would not be filled completely by the phenanthrene coke predominant in SAPO-34 and should therefore remain active for longer. A related study has been carried out on aluminosilicate zeolite materials by Park et al. [40] in which larger cage framework (erionite (ERI), zeolite-A (LTA) and UZM-5 (UFI)) were shown to deactivate more quickly than chabazite (which has the same framework structure as SAPO-34). Larger polyaromatic coke molecules were found in the large cage materials after deactivation, leading to the conclusion that chabazite can suppress formation of large polyaromatics and thereby retain activity. This is in contrast to the findings of Marcus for SAPO catalysts; however, it should be noted that the chemistry of aluminosilicate zeolites is different to that of silicoaluminophosphates.

The longer activity of SAPO-18 is also somewhat surprising in view of the differences in silicon distribution between SAPO-18 and SAPO-34 discussed in Section 2. SAPO-18 should have a lower level of acidity than SAPO-34 with the same level of silicon substitution as some of the silicon substitutes for aluminium rather than phosphorus. This might be expected to lead to quicker deactivation.

We furthermore suggest that the arrangement of the D6Rs in SAPO-18 may be more rigid than in SAPO-34. In the latter, the D6Rs are all aligned in the same direction and the flexible four-ring links allow the whole structure to expand easily in the *c*-direction. In SAPO-18, alternate cages are rotated by approximately 90° with respect to one another (Fig. 4); this means that changes to the size of the cages are restricted by the necessity of deforming the more rigid D6R units. Zeolite secondary building units [8] have been shown to be quite rigid during the negative thermal expansion of chabazite [41] and ITQ-4 [42]. Analysis of zeolite compression at high pressure is often based on the rotation of rigid units [43–47], in some cases SBUs, although Gatta and Wells have shown that the 4 = 1 SBU in erionite is not completely rigid above 2 GPa [48]. It should be noted, however, that recent work by Kapko and co-workers on hypothetical pure silica zeolite frameworks shows that the ideal AEI framework (SAPO-18) should be more flexible than the CHA framework of SAPO-34 [49].

Examination of difference Fourier maps calculated from the Rietveld refinements shows that there is a definite build-up of electron density in the cages during the reaction (Fig. 5).

We have previously used the program SQUEEZE from Spek's Platon suite [50] to provide an indication of electron density (i.e. coke molecules) in the cages for SAPO-34 [20]. However, in the case of SAPO-18, this method gave a poor indication of the electron count. This may be due to the larger number of overlapped reflections in the powder pattern of SAPO-18 compared with that of the more symmetric SAPO-34. Determining the intensity of overlapping reflections from a profile fit by the Le Bail or Pawley methods is very problematic [51].

The electron density in the cages was instead quantified by adding "dummy" carbon atoms to the Rietveld model at the positions of the highest peaks in the difference Fourier map and refining

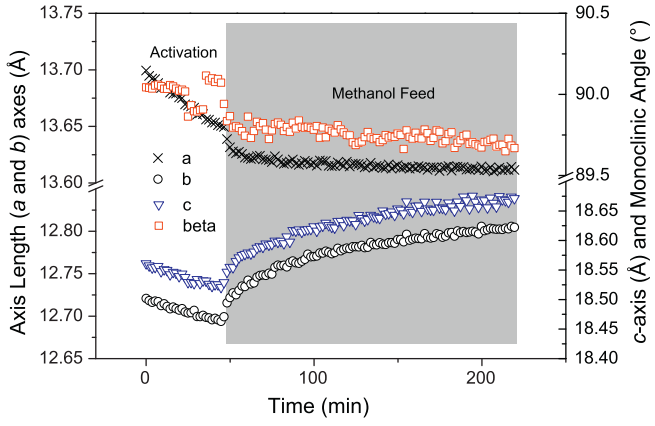

Fig. 2. Variation in the unit cell dimensions of SAPO-18 during the MTO process. Time under methanol feed is marked with a grey background. Note the negative thermal expansion during heating to 450 °C prior to the addition of methanol.

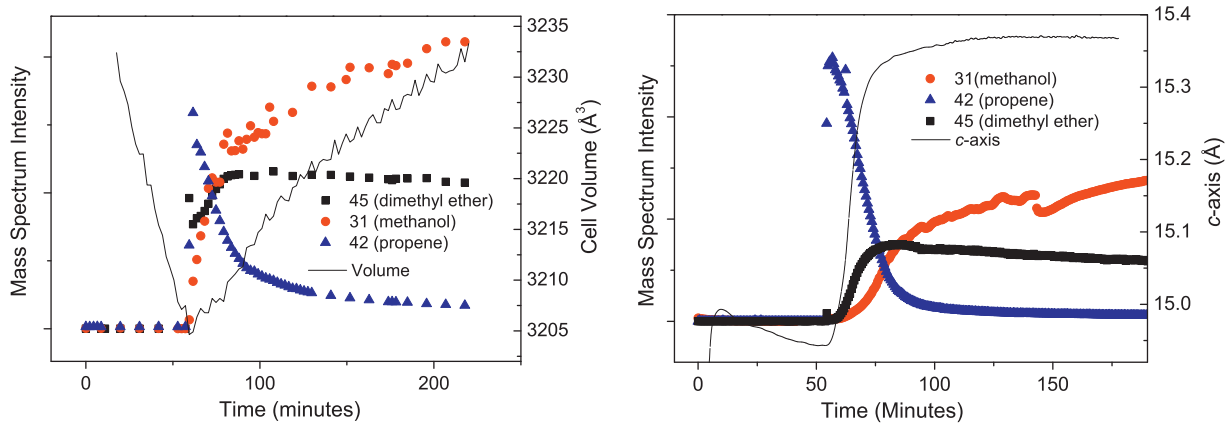

Fig. 3. Mass spectra for propene, methanol and dimethyl ether during the MTO process over SAPO-18. The propene data are multiplied by 10 to bring them onto the scale of the methanol and dimethyl ether spectra. A similar data set for SAPO-34 is shown on the right (data from [20]) – note the propene production drops almost to zero at 100 min.

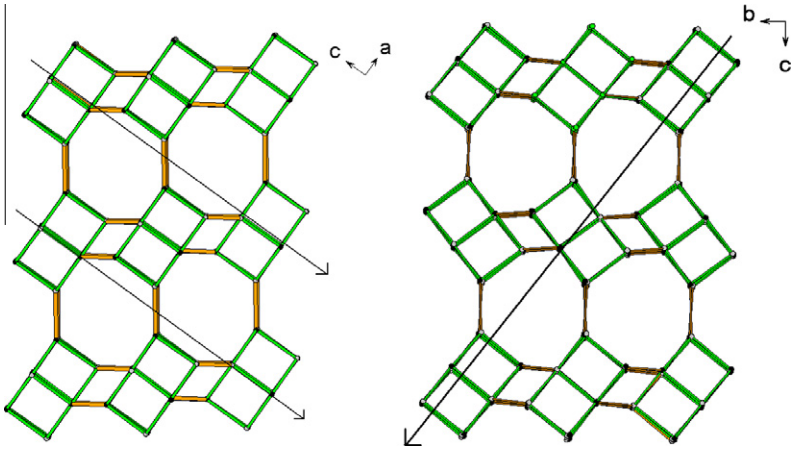

Fig. 4. The arrangement of neighbouring D6Rs SAPO-34 (left) and SAPO-18 (right), showing the alternate rotation of neighbouring D6Rs in SAPO-18 along the direction equivalent to the SAPO-34 *c*-axis (marked by a large arrow).

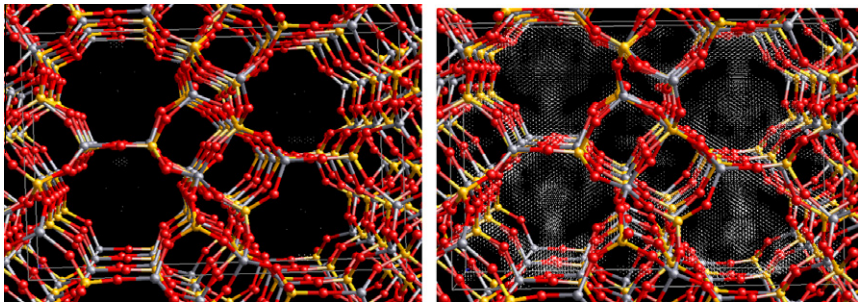

Fig. 5. Difference Fourier maps of SAPO-18 activated at 450 °C (left) and after 3 h of MTO reaction (right). Residual electron density in the channels due to MTO intermediates is visible as a yellow cloud in the right hand image. Atom colours: silver = Al, yellow = P/Si, red = oxygen. (For interpretation of the references to colour in this figure legend, the reader is referred to the web version of this article.)

their occupancies. This gave significantly improved fits for the powder patterns collected under MTO conditions, for example, data set 115 (3 h of MTO reaction) has R_{wp} (framework only) = 7.727 and R_{wp} (with dummy atoms) = 4.238. Plots of the Rietveld results are compared in Fig. 6.

Plotting the change in overall occupancy of the sites per formula unit against reaction time shows a trend which matches the shape of the unit cell volume expansion curve (Fig. 7) as previously observed for SAPO-34 [20]. Comparing the levels of site occupancy (maximum level equivalent to 8.75 electrons per formula unit for SAPO-18 after 3 h of MTO reaction) with those from similar refinements against *in situ* data for SAPO-34 under MTO conditions suggests that lower levels of electron density are present in SAPO-34 (maximum level equivalent to 6.3 electrons per formula unit at end point of the MTO reaction). It may be that still higher levels of electron density would be found in SAPO-18 after longer periods of MTO reaction – laboratory XRD data for a sample of SAPO-18 subjected to MTO reaction for 21 h show that the unit cell has expanded to a volume of 3294(5) Å^3, somewhat larger than that observed after 3 h of reaction *in situ* (3255.7(5) Å^3). Unfortunately,

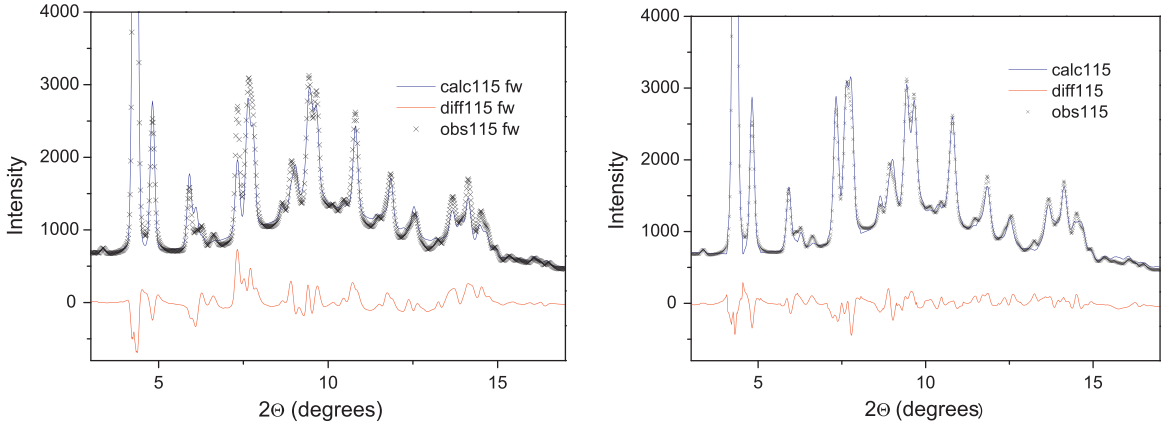

Fig. 6. Calculated, observed and difference plots of the Rietveld refinement of SAPO-18 after 3 h of MTO reaction (data set 115) for $2\theta = 3–17°$. The left refinement used only the framework as a model, while the right adds dummy carbon atoms in the cages. The most intense peak is truncated to show the changes in the less intense peaks more clearly. The small peak at $2\theta = 3.2°$ is due to a minor impurity of SAPO-5.

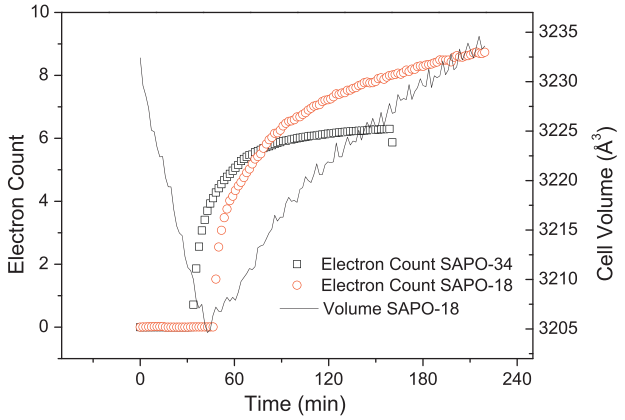

Fig. 7. Electron count from dummy atom occupancies for SAPO-18 and SAPO-34 during the MTO process. The unit cell volume of SAPO-18 is also shown to illustrate its similarity to the electron count curve.

the data were not of a sufficient quality to obtain reliable electron counts. We note that the electron counts given are only an indication of the levels of electron density present. These figures are highly dependent on the quality of fit and should only be considered approximate.

The higher electron count in SAPO-18 fits with the observation of larger coke species by Marcus et al. [17]. This does not, however, lead to increased expansion, probably because of the cage shape which allows these coke species to develop without distorting the framework. SAPO-34 also shows a clear end point in its unit cell expansion and electron count, unlike SAPO-18, although such an end point might occur after longer periods of reaction. The lack of expansion may be an indicator of why SAPO-18 remains active in the MTO process (albeit at a low level) for longer than SAPO-34. The swelling of SAPO-34 probably coincides with a fatal blocking of the pore system which appears not to occur in SAPO-18 after 3 h of reaction.

It is likely that the longer active lifetime of SAPO-18 compared with that of SAPO-34 (which occurs in spite of larger particle size) is related to the differences in structural behaviour, with the cage shape and rigid framework delaying pore blocking.

4. Conclusions

SAPO-18 behaves very differently to SAPO-34 under MTO reaction conditions. Although carbonaceous species form and reside inside the cages of SAPO-18 during the MTO process, the unit cell expands to a smaller extent than in SAPO-34 (0.9% volume expansion under MTO reaction compared with ca. 3% for SAPO-34). The smaller expansion compared with SAPO-34 (in spite of larger coke molecules being formed) can be rationalised in terms of the larger cages and more rigid D6R arrangement in SAPO-18 – the cages are not completely filled by the coke molecules present so do not expand. This is in agreement with the results of Marcus et al. [17]. The changes are related to the build-up of intermediates inside the cages as observed in difference Fourier maps; however, no quantitative relationship can be obtained as the electron counts obtained by different approaches are variable.

Acknowledgments

We thank Professor K.P. Lillerud of The University of Oslo for supplying the sample of SAPO-18; Dr Bjørnar Arstad of Sintef for discussions on SAPO-18 as an MTO catalyst, and the inGAP MTO project group for valuable input. We thank the staff of the SNBL at the ESRF for their assistance during the data collection. Professor Unni Olsbye is thanked for assistance with the conversion calculations. Funding was provided by inGAP and the Research council of Norway grant number 177320.

References

[1] C.D. Chang, J.C.W. Kuo, W.H. Lang, S.M. Jacob, J.J. Wise, A.J. Silvestri, Ind. Eng. Chem. Process Des. Develop. 17 (1978) 255–260.
[2] J. Liang, H. Li, S. Zhao, W. Guo, R. Wang, M. Ying, Appl. Catal. 64 (1990) 31–40.
[3] J. Chen, P.A. Wright, J.M. Thomas, S. Natarajan, L. Marchese, S.M. Bradley, G. Sankar, C.R.A. Catlow, P.L. Gai-Boyes, J. Phys. Chem. 98 (1994) 10216–10224.
[4] J. Chen, J.M. Thomas, P.A. Wright, R.P. Townsend, Catal. Lett. 28 (1994) 241–248.
[5] J. Chen, P.A. Wright, S. Natarajan, J.M. Thomas, in: J. Weitkamp, H. G. Karge, H. Pfeifer, W. Holderich (Eds.), Zeolites and Related Microporous Materials: State of the Art 1994, vol. 84, 1994, pp. 1731–1738.
[6] R. Wendelbo, US Pat., 5609843, 1997.
[7] R. Wendelbo, D.E. Akporiaye, A. Andersen, M.I. Dahl, H.B. Mostad, T. Fuglerud, S. Kvisle, US Pat., 6334994, 2002.
[8] C. Baerlocher, L.B. McCusker, Database of Zeolite Structures. <http://www.iza-structure.org/databases/>
[9] B. Holme, P. Cubillas, J.H. Cavka, B. Slater, M.W. Anderson, D. Akporiaye, Cryst. Growth Des. 10 (2010) 2824–2828.
[10] K.P. Lillerud, D. Akporiaye, Stud. Surf. Sci. Catal. 84 (1994) 543–550.
[11] M. Stöcker, Micropor. Mesopor. Mater. 29 (1999) 3–48.
[12] U. Olsbye, M. Bjørgen, S. Svelle, K.-P. Lillerud, S. Kolboe, Catal. Today 106 (2005) 108–111.
[13] I.M. Dahl, S. Kolboe, J. Catal. 149 (1994) 458–464.
[14] I.M. Dahl, S. Kolboe, Catal. Lett. 20 (1993) 329–336.
[15] M. Hunger, M. Seiler, A. Buchholz, Catal. Lett. 74 (2001) 61–68.
[16] A. Buchholz, W. Wang, M. Xu, A. Arnold, M. Hunger, Micropor. Mesopor. Mater. 56 (2002) 267–278.

[17] D.M. Marcus, W. Song, L.L. Ng, J.F. Haw, Langmuir 18 (2002) 8386–8391.
[18] A.G. Gayubo, R. Vivanco, A. Alonso, B. Valle, A.T. Aguayo, Ind. Eng. Chem. Res. 44 (2005) 6605–6614.
[19] A.T. Aguayo, A.G. Gayubo, R. Vivanco, M. Olazar, J. Bilbao, Appl. Catal. A: Gen. 283 (2005) 197–207.
[20] D.S. Wragg, R.E. Johnsen, M. Balasundaram, P. Norby, H. Fjellvåg, A. Grønvold, T. Fuglerud, J. Hafizovic, Ø.B. Vistad, D. Akporiaye, J. Catal. 268 (2009) 290–296.
[21] D.S. Wragg, R.E. Johnsen, P. Norby, H. Fjellvåg, Micropor. Mesopor. Mater. 134 (2010) 210–215.
[22] G. Sastre, D.W. Lewis, C.R.A. Catlow, J. Mol. Catal. A: Chem. 119 (1997) 349–356.
[23] P. Norby, J. Am. Chem. Soc. 119 (1997) 5215–5221.
[24] A.P. Hammersley, S.O. Svensson, M. Hanfland, A.N. Fitch, D. Hausermann, High Pressure Res. 14 (1996) 235–248.
[25] A.P. Hammersley, 2004. <http://www.esrf.eu/computing/scientific/FIT2D/>.
[26] A. Le Bail, H. Duroy, J.L. Fourquet, Mater. Res. Bull. 23 (1988) 447–452.
[27] G.S. Pawley, J. Appl. Crystallogr. 14 (1981) 357–361.
[28] A.C. Larson, R.B. Von Dreele, Los Alamos National Laboratory Report LAUR, 1994, pp. 86–74.
[29] [29] A.A. Coelho, TOPAS V4.1, Bruker AXS, 2006.
[30] G.W. Stinton, J.S.O. Evans, J. Appl. Crystallogr. 40 (2007) 87–95.
[31] M. Amri, R.I. Walton, Chem. Mater. 21 (2009) 3380–3390.
[32] M.G. Abraha, X. Wu, R.G. Anthony, in: G.F. Froment, K.C. Waugh (Eds.), vol. 133, Elsevier, 2001, pp. 211–218.
[33] I.M. Dahl, R. Wendelbo, A. Andersen, D. Akporiaye, H. Mostad, T. Fuglerud, Micropor. Mesopor. Mater. 29 (1999) 159–171.
[34] B.P.C. Hereijgers, F. Bleken, M.H. Nilsen, S. Svelle, K.-P. Lillerud, M. Bjørgen, B.M. Weckhuysen, U. Olsbye, J. Catal. 264 (2009) 77–87.
[35] N. Nishiyama, M. Kawaguchi, Y. Hirota, D. Van Vu, Y. Egashira, K. Ueyama, Appl. Catal. A: Gen. 362 (2009) 193–199.
[36] S. Wilson, P. Barger, Micropor. Mesopor Mater. 29 (1999) 117–126.
[37] S.T. Wilson, R.W. Broach, C.S. Blackwell, C.A. Bateman, N.K. McGuire, R.M. Kirchner, Micropor. Mesopor. Mater. 28 (1999) 125–137.
[38] J.M. Bennett, R.M. Kirchner, S.T. Wilson, Stud. Surf. Sci. Catal. 49 (1989) 731–739.
[39] N.K. McGuire, C.A. Bateman, C. Scott Blackwell, S.T. Wilson, R.M. Kirchner, Zeolites 15 (1995) 460–469.
[40] J.W. Park, J.Y. Lee, K.S. Kim, S.B. Hong, G. Seo, Appl. Catal. A: Gen. 339 (2008) 36–44.
[41] D.A. Woodcock, P. Lightfoot, L.A. Villaescusa, M.J. Diaz-Cabanas, M.A. Camblor, D. Engberg, Chem. Mater. 11 (1999) 2508–2514.
[42] L.A. Villaescusa, P. Lightfoot, S.J. Teat, R.E. Morris, J. Am. Chem. Soc. 123 (2001) 5453–5459.
[43] S.A. Wells, M.T. Dove, M.G. Tucker, J. Phys.: Condens. Matter 14 (2002) 4567–4584.
[44] S.A. Wells, M.T. Dove, M.G. Tucker, K. Trachenko, J. Phys.: Condens. Matter 14 (2002) 4645–4657.
[45] K.D. Hammonds, H. Deng, V. Heine, M.T. Dove, Phys. Rev. Lett. 78 (1997) 3701–3704.
[46] M.T. Dove, M. Gambhir, K.D. Hammonds, V. Heine, A.K.A. Pryde, Phase Transit. 58 (1996) 121–143.
[47] M.T. Dove, V. Heine, K.D. Hammonds, Mineral. Mag. 59 (1995) 629–639.
[48] G.D. Gatta, S.A. Wells, Phys. Chem. Miner. 31 (2004) 465–474.
[49] V. Kapko, C. Dawson, M.M.J. Treacy, M.F. Thorpe, Phys. Chem. Chem. Phys. 12 (2010) 8531–8541.
[50] A.L. Spek, Utrecht University, Utrecht, The Netherlands, 2008.
[51] Caliandro, C. Giacovazzo, R. Rizi, in: R.E. Dinnebier, S.J.L. Billinge (Eds.), Powder Diffraction: Theory and Practice, Royal Society of Chemistry, Cambridge, 2008, pp. 227–265.